Ordering of apolar and polar solutes in nematic solvents

T. Dingemans
ICASE Structures and Materials, NASA Langley Research Center, Hampton, Virginia 23681-2199

D. J. Photinos
Department of Materials Science, University of Patras, Patras 26500, Greece

E. T. Samulski
Department of Chemistry, University of North Carolina at Chapel Hill, Chapel Hill, North Carolina 27599-3290

A. F. Terzis[a)]
Department of Physics, University of Patras, Patras 26500, Greece

C. Wutz
Institut fur Technische und Makromolekulare Chemie, D-20146 Hamburg, Germany

(Received 17 September 2002; accepted 24 January 2003)

The quadrupolar splittings of deuteriated para- and ortho-dichlorobenzene (1,4-DCB and 1,2-DCB, respectively) are measured by nuclear magnetic resonance (NMR) in the nematic solvents hexyl- and pentyloxy-substituted diphenyl diacetylene (DPDA-C6 and DPDA-OC5, respectively). Measurements are taken for all four combinations of the nominally apolar (1,4-DCB) and polar (1,2-DCB) solutes in the apolar (DPDA-C6) and polar (DPDA-OC5) solvents, and throughout the entire nematic temperature range of the solutions. The temperature dependence of the second-rank orientational order parameters of the solutes are obtained from these measurements and the respective order parameters of the mesogenic cores of solvent molecules are obtained independently from carbon-13 NMR measurements. The order parameter profiles of the two solutes are found to be very different but show little variation from one solvent to the other. The results are analyzed and interpreted in terms of the underlying molecular interactions using atomistic solvent–solute potentials. The influence of electrostatic interactions on solute ordering is directly evaluated by computing the order parameters with and without the electrostatic component of the atomistic potential. It is observed to be small. It is also found that the important interactions in these solvent–solute systems are operative over short intermolecular distances for which the representation of the partial charge distributions in terms of overall molecular dipole and quadrupole moments is not valid. [DOI: 10.1063/1.1560941]

I. INTRODUCTION

For more than three decades researchers have been intrigued by the nature of the orientational order that characterizes the unusual fluid phase of matter known as the liquid crystalline (LC) state. In the mid 1960s nuclear magnetic resonance (NMR) was found to be an ideal technique for determining the orientational order of solutes dissolved in nematic LCs; second-rank NMR nuclear dipolar and quadrupolar interactions are incompletely averaged in nematics.[1] Moreover, as the residual proton dipolar interactions are rigorously related to the solute's geometry, LC-NMR became a tool for structure determination in a fluid phase[2] and this application has dominated the last four decades of LC-NMR studies.[3] Concomitantly, the quadrupolar interactions exhibited by deuterium-labeled, small, symmetric, ''guest'' molecules were effectively used to map out the phase symmetries and orientational order in liquid crystal ''hosts'' for both types of thermotropic liquid crystals, prolate-shaped (calamitic) liquid crystals,[4] and oblate-shaped (discotic) liquid crystals.[5] In the case of lyotropic liquid crystals, both probes and deuterium-labeled amphiphiles were used to characterize the orientational order in the aliphatic strata in lamellar phases.[6] These indirect uses of NMR evolved into investigations of the probe molecule's orientation mechanism and NMR became the method of choice for characterizing the anisotropic mean field in liquid crystals.[7] For completeness, it should be noted that dynamical processes in liquid crystals have unique characteristics also, and NMR has played a key role in that area.[8]

Currently, apart from contemporary protein structure refinement applications,[9] the primary use of LC-NMR is focused on studies designed to show which intermolecular interactions determine the average orientation of simple probe solutes dissolved in nematic solvents. The focus on probes continues because of practical considerations: mesogens are too complex to elicit the details required for constructing mesogen–mesogen intermolecular interaction potentials from LC-NMR data. In the interim, the much simpler class

a)Author to whom correspondence should be addressed. Electronic mail: terzis@physics.upatras.gr; Tel.: (+30) 2 610-997 618; Fax: (+30) 2 610-997 618.

of solutes has been employed to study the mechanism of molecular orientation in nematics. Judiciously chosen solutes, ranging from diatomics to flexible alkanes, have been modeled with increasingly sophisticated models.[7,10,11] Extension of such modeling is anticipated to result in a more detailed understanding of the nature of intermolecular interactions in LCs and ultimately to enable one to predict structure–property relations, namely, how a mesogen's molecular structural features are manifested in its LC phase stability and phase type. It is in this spirit that we study the orientational order of two solutes 1,4-dichlorobenzene and 1,2-dichlorobenzene, nominally ''apolar'' and ''polar'' molecules, in two nematic solvents with LC-NMR. The goal is to refine our understanding of the relative importance of the various contributions to the solute–solvent interaction potential, U. We apply contemporary modeling—both solute and solvent molecules are treated in atomistic detail—to construct U and have the option of ''turning-off'' the charge distributions on both solute and mesogen in order to assess directly the effects of electrostatic interactions on solute orientational ordering.

It is generally accepted that molecular shape dominates solute ordering in nematics,[12,13] and a variety of models have been explored for computing the magnitude of this steric, short-range, interaction.[10–13] However, there are clear cases where electrostatic interactions are also important[11] and generally, it is instructive to gauge the importance of steric interactions relative to the electrostatic contributions to solute ordering. Recently the role of electrostatic interactions in solute ordering has been described as a major unsolved problem—a ''holy grail'' of liquid crystal physics.[14] This is not the point of view we advocate here. We show that electrostatic interactions are convolved with the excluded volume interactions, that their influence on the ordering of the solutes studied is weaker than that of the excluded volume interactions, but nevertheless can be evaluated consistently and reasonably accurately starting from the explicit atomistic solvent–solute potential.

Strictly, a complete description of the electrostatic interactions in liquid crystals requires the partial charge distribution on each molecule to be determined as a function of its conformation and of its configuration relative to the other molecules surrounding it. This, in turn, could be accomplished in principle given the partial charge distribution for the free molecule and given the polarisabilities of the molecular segments. The latter allow the deformations of the charge distribution of the interacting molecule to be determined. Such a description, however, entails the use of potentials that are not pairwise additive and, to our knowledge, has not been attempted in any theoretical or computer simulation studies of liquid crystals to date.

Considerable simplification is brought about if the partial charge distribution on the molecular segments is treated as fixed, i.e., by ignoring molecular polarizability altogether, since this renders the intermolecular electrostatic potential pairwise additive. In practice, modeling usually goes one simplifying step further and replaces the partial charge distribution by the leading terms of its multipole expansion. The electrostatic interactions are thus represented as originating from a set of permanent dipole or quadrupole moments fixed on the molecular frame. An obvious flaw of this representation is that, since the multipole expansion is valid only for distances that are large compared to the spatial extent of the charge distribution, the leading-moment potential may severely deviate from the actual partial charge potential at short intermolecular separations, even in the absence of any polarizability effects. Furthermore, the multipole expansion of a charge distribution is not unique in that it is done with respect to an arbitrarily defined origin. However, aside from computational simplification, there are advantages of conceptual clarity in using the multipole expansion, particularly when addressing such fundamental issues as the possible residual effects of polar interactions in apolar media. In such cases, where the focus is not on quantitative accuracy, it is appropriate to isolate the polar part of the charge distribution and represent it by a dipole moment. In fact, a question that has been posed in many recent studies concerns the effect of the electrostatic polarity of the molecules on ordering, both in apolar and in polar LC phases. In some of the early attempts to interpret NMR experiments on dipolar solutes in common (apolar) nematic solvents, a naive picture of the nematic medium was used according to which any dipolar interactions between solvent and solute molecules are averaged out by virtue of the apolarity of the nematic medium.[10,15,16] In this naive picture, the leading-rank electrostatic interactions felt by a solute molecule in a nematic solvent are associated with the electric quadrupole moment of the solute molecule which is assumed to couple to an ad hoc property of the nematic medium bearing the physical dimensions of an electric field gradient (EFG). This picture was soon demonstrated to be inadequate[17,18] and it is now well established by several theoretical works and numerous computer simulations[19–23] that residual dipolar interactions are not only present in apolar mesophases, nematic, smectic or columnar, but that they can also have substantial effects on the thermodynamic stability of these phases,[24] produce molecular dimerisation via dipolar association,[25,26] give rise to phase re-entrance phenomena,[27] cause structural modifications in smectics,[28,29] etc. On the other hand, it was demonstrated theoretically,[11] and later found in simulations,[30] that the ad hoc ''EFG of the solvent'' is not strictly a solvent property but depends on the structure of the solute molecules as well. Moreover, the notion of a solvent-characteristic EFG is proven inadequate to account for direct NMR measurements of average EFGs experienced by the quadrupolar nuclei of the noble gas isotopes ^{21}Ne, ^{83}Kr, and ^{131}Xe in nematic solvents.[31] For the interpretation of these measurements it is necessary to include, in addition to the ''solvent EFG,'' at least one more source of EFG, and also assume that the ''solvent EFG'' is solute dependent.

Herein we illustrate the relative importance of electrostatic interactions by analyzing LC-NMR data for a pair of polar and apolar solutes that are structural isomers, ortho- and para-dichlorobenzene, respectively, dissolved in polar and apolar nematogens. The latter liquid crystals are the symmetric calamitic mesogens, hexyl- and pentyloxy-substituted diphenyl diacetylenes, DPDA-OC5 and DPDA-C6, respectively (see Scheme 1).

Scheme 1. Chemical structure of apolar (DPDA-C6) and polar (DPDA-OC5) solvents.

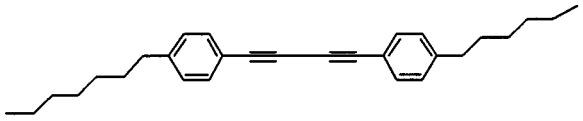

4,4'-di-*n*-hexyldiphenyldiacetylene **(DPDA-C6)**

4,4'-di-(*n*-pentyloxy)diphenyldiacetylene **(DPDA-O-C5)**

These two mesogens differ only in the linkage of the equivalent-length, terminal tails to the mesogenic core. Thus, it seems reasonable to conjecture that the DPDA-OC5 mesogen might exhibit specific electrostatic contributions to solute ordering due to the charge density associated with its ether linkages; DPDA-C6 is devoid of heteroatoms and of significant electrostatic charge density differences from atom to atom. It is difficult to probe the role of such subtle structural differences on solute ordering if the modeling of intermolecular interactions is too coarse—either uniaxial continuum descriptions of the nematic solvent[10,14] or even approximate solute shapes (spherocylinders, ellipsoids, etc.) endowed with electrostatic moments.[11] We therefore perform straightforward atomistic calculations of the solute–solvent interactions for all relative orientations using conventional force fields (Dreiding force field).[32] This enables us to construct the solvent–solute interaction potential U and the solute orientational distribution function $f(\omega)$ in these two nematics. While the calculations confirm the dominance of the short-range repulsive contributions, by performing the same atomistic calculations with the electrostatic interactions suppressed we can estimate the relative importance of excluded volume and electrostatic interactions to solute ordering for the two solutes ortho-dichlorobenzene (1,2-DCB) and para-dichlorobenzene (1,4-DCB).

II. BACKGROUND

LC-NMR has been routinely used to study how both the mesogens themselves and solute probe molecules are oriented by a ''potential of mean torque,'' $V(\omega)$, characterizing the LC medium's anisotropic mean field; ω represents the generalized angular variables and is referenced to the nematic director **N** (herein assumed parallel to the spectrometer magnetic field). The initial focus of LC-NMR studies was on determining solute geometry from resolved proton dipole–dipole hyperfine couplings,[3,8] D_{ij}, which in turn, are related to the solute's (vibrationally-averaged) internuclear distances, r_{ij},

$$D_{ij} \approx \frac{\gamma_i \gamma_j}{r_{ij}^3} \langle 3\cos^2(\theta_{ij}) - 1 \rangle / 2 = \frac{\gamma_i \gamma_j}{r_{ij}^3} \sum_{ab} \cos\theta_a \cos\theta_b S_{ab}. \quad (1)$$

Here θ_{ij} is the time-dependent angle prescribed by r_{ij} and the magnetic field. Clearly, a prerequisite for extracting the solute geometry r_{ij} from measured couplings is an independent determination of the average degree of orientation of the interaction direction.

Similarly for deuterium NMR, the incompletely averaged electric field gradient at the nucleus results in quadrupolar splittings $\Delta\nu_i$ that depend on the average orientation of the C–D bonds relative to the magnetic field,[33]

$$\Delta\nu_i \approx e^2 q_i Q \langle 3\cos^2(\theta_i) - 1 \rangle / 2 = e^2 q_i Q \sum_{ab} \cos\theta_a \cos\theta_b S_{ab}. \quad (2)$$

The averaged orientation of the interaction direction is related to the solute molecule's orientational order via the angle θ_i locating the direction of the C–D bond relative to the magnetic field. The direction cosines of the interaction direction (internuclear vector $\mathbf{r}_{ij}$ or electric field gradient along the C–D bond) in a Cartesian, solute-fixed, axis frame a,b,c are denoted by $\cos\theta_a$. The solute order parameters S_{ab} appearing in Eqs. (1) and (2) are the elements of the traceless ordering matrix of the solute and can be obtained as the rank 2 moments of the solute's orientational distribution function, $f(\omega)$, according to the defining relations,

$$S_{ab} = \frac{1}{2} \int d\omega f(\omega) [3(\mathbf{a}\cdot\mathbf{N})(\mathbf{b}\cdot\mathbf{N}) - 1], \quad (3)$$

where **a**, **b** correspond to the unit vectors along the axes of the solute-fixed molecular frame. The orientational distribution function of the solute is related to the potential of mean torque $V(\omega)$ as follows:[34]

$$f(\omega) = \frac{\exp\left(-\frac{V(\omega)}{k_B T}\right)}{\int d\omega \exp\left(-\frac{V(\omega)}{k_B T}\right)}. \quad (4)$$

Quite generally, the potential of mean torque felt by a solute molecule in a uniaxial nematic solvent can be expanded in spherical harmonics $Y_{lm}(\omega)$ of even rank l. The coefficients in this expansion are related to the solute–solvent interaction potential but a rigorous closed form of this relation cannot be obtained for any system of practical interest. It is therefore necessary to resort to approximation schemes in order to relate in closed form the expansion coefficients to the interaction potential. Here we use an approximation scheme that is based on the variational cluster method for pairwise additive interactions and has been described in Refs. 11 and 13. Briefly, the approximation consists in neglecting the correlations among the solvent molecules and using renormalized densities in order to partly compensate for the neglected correlations. This leads to the following form for the spherical harmonic expansion of the potential of mean torque acting on the solute molecules,

$$V(\omega)/k_B T = \overline{\rho} C_{00}(T^*) \sum \frac{C_{lm}}{C_{00}(T^*)} \langle P_l \rangle \left[1 - \frac{\delta_{lm}}{2}\right] \times [Y_{lm}(\omega) + Y_{lm}^*(\omega)]. \quad (5)$$

Here $\overline{\rho}$ denotes the effective (renormalized) particle density of the solvent (number of solvent molecules per unit volume of the solution) and $\langle P_l \rangle$ are the lth rank order parameters of the solvent (assumed to be of negligible molecular biaxiality). The coefficients C_{lm} are given by

$$C_{lm} = \frac{1}{2} \int \int d\mathbf{r} d\omega [1 - e^{-U/k_B T}][Y_{lm}(\omega) + Y^*_{lm}(\omega)], \tag{6}$$

where U is the interaction potential between the solute and the solvent and the integration is over all solute–solvent separations ($\mathbf{r}$) and relative orientations (ω). In order to have dimensionless expansion in Eq. (5), all the coefficients are expressed in units of the isotropic coefficient C_{00}, which, according to Eq. (6) is given by

$$C_{00}(T^*) = \frac{1}{8\pi^2} \int \int d\mathbf{r} d\omega [1 - e^{-U/k_B T^*}], \tag{7}$$

where T^* is a fixed reference temperature.

The solute–solute interactions do not appear in the expression of Eq. (5) since the concentration of solute molecules in the nematic solution is assumed negligibly small. Furthermore, the solvent–solvent interactions enter indirectly through the order parameters $\langle P_l \rangle$ of the solvent molecules. Accordingly, the solute potential of mean torque in Eq. (5), and thereby the solute order parameters in Eq. (3), can be fully determined given the solvent effective density $\overline{\rho}$, order parameters $\langle P_l \rangle$, and the detailed solvent–solute potential. The atomistic evaluation of the latter is outlined in Sec. IV.

III. EXPERIMENT

A. Materials

In order to probe the role of electrostatic solute–solvent interactions we use nematic solvents having minimal structural differences between a polar and an apolar solvent. We have synthesized two very simple nematogens that are structurally isomorphous: alkyl- and alkyloxy-substituted diphenyl diacetylene (DPDA) liquid crystals. The synthetic details and thermal properties are reported in the Appendix. Both DPDA mesogens (see Scheme 1) are symmetric and have typical calamitic tail–core–tail structures with the same number of (united) atoms in the terminal chains. Initially reported by Grant,[35,36] DPDA liquid crystals have several properties which make them ideally suited for NMR studies; positive diamagnetic susceptibility and the ability to form stable, low viscosity, nematic phases with accessible temperature ranges ($<160\,°C$). The pentyloxy derivative, DPDA-OC5, differs from the apolar hexyl derivative, DPDA-C6, in that there is a nonuniform charge density in the tails associated with the ether linkages to the diphenyl diacetylene mesogenic core. DPDA-C6 was reported by Grant[35,36] and has a nematic range from 58.6 to 85.3 °C; DPDA-OC5 exhibits a nematic phase between 122–159 °C and is believed to be a new liquid crystal. Separated local field NMR (SLF NMR) spectroscopy was used to determine the temperature dependence of each mesogen's orientational order parameters across the respective nematic ranges.

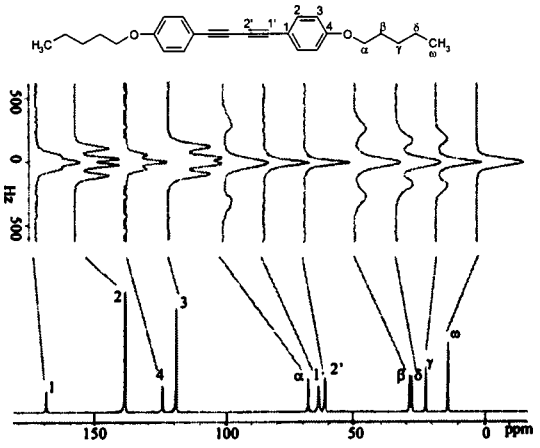

FIG. 1. Projection in ^{13}C dimension of the 2D-SLF spectrum of DPDA-OC5 at 306 K and the corresponding C–H multiplet for each carbon assigned by numbers.

We present the results of deuterium LC-NMR studies of solvent–solute effects using two solutes of very simple molecular structure, 1,4-dichlorobenzene-d_4 (1,4-DCB) and 1,2-dichlorobenzene-d_4 (1,2-DCB), in the DPDA-C6 and DPDA-OC5 solvents. These solutes have been considered before as potential probes of dipole-induced ordering in so-called zero-electric-field-gradient nematic mixtures, but it was concluded that permanent dipoles have a negligible influence on solute orientation.[14]

B. Mesogen order parameters

All of the NMR experiments were carried out on a Bruker Avance 360 NMR spectrometer with a Bruker CP/MAS probe (4 mm rotor). The carbon–proton coupling constants of the DPDA samples were measured using the separated local field (SLF) with off-magic-angle spinning technique.[37] During the evolution period (t_1), proton–proton dipolar couplings were removed by applying a windowless homonuclear dipolar decoupling pulse sequence (BLEW-48),[38] so that exclusively carbon–proton dipolar couplings were retained. The high resolution carbon-13 spectrum was acquired during the t_2 period using a WALTZ-16 pulse sequence for proton decoupling. In order to avoid sample heating by high decoupling power, the samples were spun at an angle of $\theta = 49.0°$, which is slightly smaller than the magic angle (54.7°). This off-magic-angle spinning technique reduces the dipolar couplings by a factor of $(3\cos^2\theta - 1)/2$.[39]

It has been demonstrated in Ref. 40 that carbon-13 SLF NMR spectroscopy provides carbon–proton dipolar coupling constants for each carbon exhibiting a resolved resonance. As an example, Fig. 1 displays the projection in the ^{13}C dimension of the 2D-SLF spectrum of DPDA-OC5 and the corresponding C–H multiplet for each carbon as assigned to the chemical structure in the figure inset.

From the signals of the aromatic carbons in the chemical shift range between 170 and 120 ppm, the orientational order of the mesogenic core of the molecule can be determined.

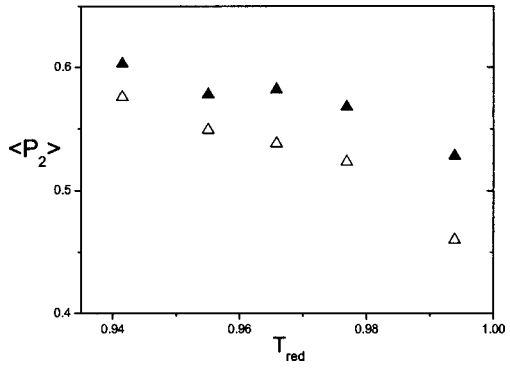

FIG. 2. Order parameters $\langle P_2\rangle(\equiv S_{zz})$ evaluated according to Eq. (8) from the experimental data on dipolar C–H coupling constants for DPDA-C6 (open triangles) and DPDA-OC5 (filled triangles) as a function of the reduced temperature.

The phenylene rings in the DPDA molecule have D_2 symmetry. Therefore, the dipolar coupling constant for each C–H spin pair is given by

$$D_{\mathrm{CH}}=\frac{\gamma_{\mathrm{C}}\gamma_{\mathrm{H}}}{2r_{\mathrm{CH}}^3}\cdot[(3\cos^2\theta_{\mathrm{CH}_z}-1)S_{zz}+(\cos^2\theta_{\mathrm{CH}_x}-\cos^2\theta_{\mathrm{CH}_y})(S_{xx}-S_{yy})], \quad (8)$$

where γ_{C} and γ_{H} are the gyromagnetic ratios for carbon and hydrogen, r_{CH} is the internuclear distance between carbon and proton, and $\theta_{\mathrm{CH}_\alpha}$ is the angle between r_{CH} and the molecular fixed α-axis. In the chosen molecule-fixed *x,y,z*-frame, *z* is the twofold axis of the phenylene rings and *x* lies in the ring plane perpendicular to *z*. Ideal hexagonal ring geometries were used with C–C and C–H bond lengths 1.40 and 1.08 Å, respectively. The order parameters of the phenylene rings in the rigid core of the molecule (S_{zz} and $S_{xx}-S_{yy}$) were obtained by least square fits of the calculated C–H dipolar coupling constants to the experimental data. Figure 2 shows the order parameter $S_{zz}\equiv\langle P_2\rangle$ of DPDA-C6 and DPDA-OC5 as a function of the reduced temperature $T_{\mathrm{red}}=T/T_{\mathrm{NI}}$. The biaxial order parameter $(S_{xx}-S_{yy})$ (not depicted) is close to zero indicating a virtually uniaxial average mesogen structure. The S_{zz} parameters reveal that the orientational order of both liquid crystals increases, as expected, with decreasing temperature; DPDA-OC5 exhibits higher orientational order than DPDA-C6.

C. Deuterium quadrupolar splittings and order parameters of the solutes

We studied 2% solutions of fully deuteriated 1,4-DCB and 1,2-DCB in the nematic solvents. The multiline spectrum of 1,4-DCB [Fig. 3(a)] results from the combination of identical quadrupolar splittings of the four equivalent C–D bonds ($\Delta\nu$) and the dipolar couplings (D) among adjacent deuteron pairs (along the *a*-axis).[41,42] The spectrum of 1,2-DCB [Fig. 3(b)] consists of two doublets ($\Delta\nu_1,\Delta\nu_2$) from the two distinct C–D bond orientations (the 3,6- and 4,5-deuterons of 1,2-dichlorobenzene-d_4). The outer doublet can be assigned

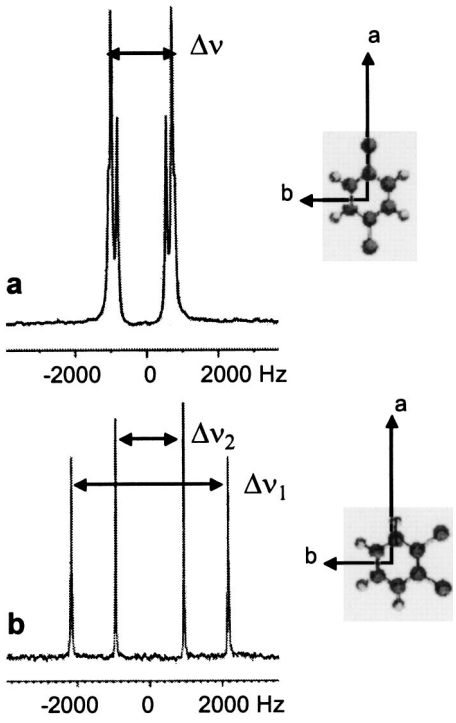

FIG. 3. ^{2}H-NMR spectra of dichlorobenzene solutes in the nematic phase of DPDA-C6 at 80 °C. (a) 1,4-DCB-d_4 exhibits dipolar fine structure superposed on the quadrupolar splitting $\Delta\nu$. (b) 1,2-DCB-d_4 exhibits two quadrupolar splittings $\Delta\nu_1$ and $\Delta\nu_2$ corresponding to the distinguishable 3,6 and 4,5 deuterons. (Inset) Molecular fixed *a,b,c*-axes on the DCB solutes.

to the C–D bonds adjacent to the chlorine atoms based on the 4 Hz down field shift of its center (chemical shift) relative to the inner doublet.

The measured values of the quadrupolar splittings are plotted as a function of reduced temperature $T_{\mathrm{red}}\equiv T/T_{\mathrm{NI}}$ in Fig. 4(a). It is apparent from these plots that the splittings of the two solutes are much different in magnitude and exhibit opposite temperature dependencies; large splittings decreasing with increasing temperature for 1,2-DCB and small splittings, increasing with temperature, for 1,4-DCB. Furthermore, while the splittings of 1,4-DCB are somewhat smaller in the DPDA-C6 than in the DPDA-OC5 solvent at all temperatures, the splittings of 1,2-DCB are nearly identical in the two solvents.

At first sight, the apparent lack of an appreciable ''solvent effect'' in the splittings of the 1,2-DCB might suggest that the interactions of the solute molecules with the molecules of the two different solvents are practically identical. However, if proper account is taken of the fact that the two solvents have different order parameters at the same reduced temperature, as seen on the plots of Fig. 2, one is led to the opposite conclusion: since one solvent is more ordered than the other and the splittings of the solute are nearly equal in the two solvents, then the orientational correlations among solute–solvent molecules must be weaker in the more ordered solvent (DPDA-OC5). The plots of Fig. 4(a) reflect the combined effect on solute ordering of both the degree of order in the solvent (determined by the solvent–solvent interactions) and the strength of the orientational coupling of

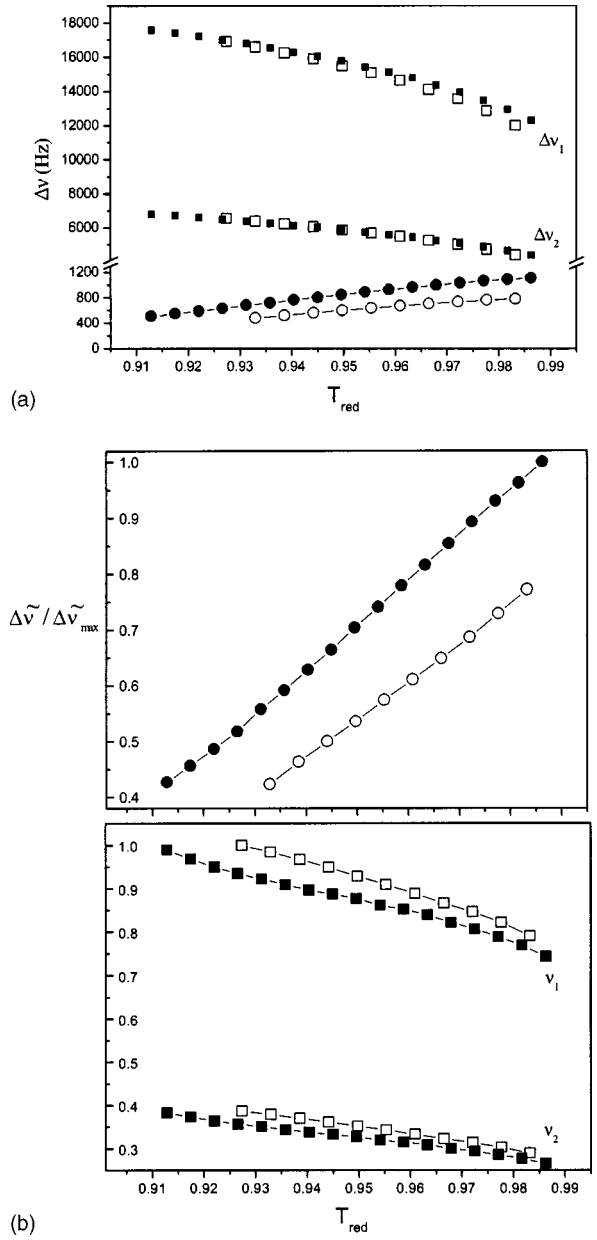

FIG. 4. (a) Plots of the temperature dependence of experimental quadrupolar splittings of the 1,4-DCB (circles) and the 1,2-DCB (squares) solutes in the nematic solvents DPDA-OC5 (filled symbols) and DPDA-C6 (open symbols). (b) Plots of the experimental quadrupolar splittings of (a) after dividing by the value of the order parameter of the respective solvent (see Fig. 2). The reduced splittings are plotted on a relative scale where the largest entry is assigned the value 1. The symbols are as in (a).

the solute molecules to the solvent (determined by solvent–solute interactions). For the purpose of comparing the strength of solvent–solute orientational coupling in the two solvents it is more appropriate to compare not directly the splittings $\Delta\nu_i$ but their scaled values with respect to the solvent order parameter $\langle P_2\rangle$. These scaled splittings $\Delta\tilde{\nu}_i = \Delta\nu_i/\langle P_2\rangle$ are plotted in Fig. 4(b).

As seen in these plots, the scaled splittings are clearly different in the two solutes. The ordering of 1,2-DCB is seen to be stronger in DPDA-C6 compared to its ordering in DPDA-OC5 *for the same value of solvent order parameter*. The ordering of 1,4-DCB remains stronger in DPDA-OC5, as suggested by the measured values of the splittings in Fig. 4(a), but the scaling of the splittings in Fig. 4(b) reduces somewhat the difference between the two solvents since the large splittings (corresponding to the DPDA-OC5 solvent) are divided by the larger value of solvent order parameter $\langle P_2\rangle$.

By choosing the appropriate solute-fixed *a,b,c*-frame (see Fig. 3, inset), the traceless order matrix of the rigid solutes contains exclusively diagonal elements. Generally, the incompletely averaged nuclear spin interaction is related to a sum over the relevant order parameters and associated direction cosines defining the interaction direction in the solute-fixed *a,b,c*-frame [see Eq. (2)]. In the axis system employed—the *c*-axis normal to the solute ring and the *a*- and *b*-axes in the ring plane with *a* along the *para* twofold symmetry axis of 1,4-DCB (see Fig. 3 inset)—S_{ab} is diagonal and one finds, for an idealized solute geometry and no asymmetry in the C–D bond electric field gradient tensor, that the quadrupolar splitting for 1,4-DCB is given by

$$\begin{aligned}\Delta\nu &= \tfrac{3}{2}e^2qQ[\cos^2\theta_a S_{aa} + \cos^2\theta_b S_{bb}]\\ &= \tfrac{3}{2}e^2qQ[\tfrac{1}{4}S_{aa} + \tfrac{3}{4}S_{bb}].\end{aligned} \tag{9}$$

In the case of the 1,2-DCB solute there are two distinct quadrupolar interaction directions in the solute-fixed *a,b,c*-frame (see Fig. 3) and we find for an ideal solute geometry a pair of quadrupolar splittings,

$$\begin{aligned}\Delta\nu_1 &= \tfrac{3}{2}e^2qQS_{aa},\\ \Delta\nu_2 &= \tfrac{3}{2}e^2qQ[\tfrac{1}{4}S_{aa} + \tfrac{3}{4}S_{bb}].\end{aligned} \tag{10}$$

Hence, the solute ordering in both solvents—the relevant order parameters $(S_{aa}-S_{bb})$ and S_{cc}—can be evaluated from the observed quadrupolar splittings. The result of the order parameters calculated directly from the experimental splittings are shown in Fig. 5. Due to the sign ambiguity of the measured coupling constants—generally, only $|\Delta\nu|$ and $|D|$ can be determined—a unique set of S_{aa}, S_{bb}, and S_{cc} order parameters cannot be evaluated directly from LC-NMR spectra. As an example, we show such data sets for 1,4-DCB and 1,2-DCB each in the nematic solvent DPDA-C6 (Table I). The modeling we use in this work identifies the bold-face entries in Table I as those corresponding to the actual solute order parameters.

It is evident in the plots of Fig. 5 that the qualitatively different temperature dependence of the splittings of the two solutes is reflected in the temperature dependence of the order parameters: $(S_{aa}-S_{bb})$ has opposite sign for the two solutes while S_{cc} is very small and nearly constant for 1,2-DCB as opposed to 1,4-DCB for which it has a fairly large magnitude, increasing with decreasing temperature. Finally, the accidental near coincidence of the splittings of 1,2-DCB in the two solvents is naturally carried over to the respective order parameter plots. As in the case of Fig. 4(a), it should be kept in mind that the solute order parameter plots of Fig. 5 allow comparisons at the same value of solvent reduced temperature but not at the same value of the solvent order parameter. On the other hand, the values of order parameters obtained for 1,4-DCB in the two solvents are nearly identical

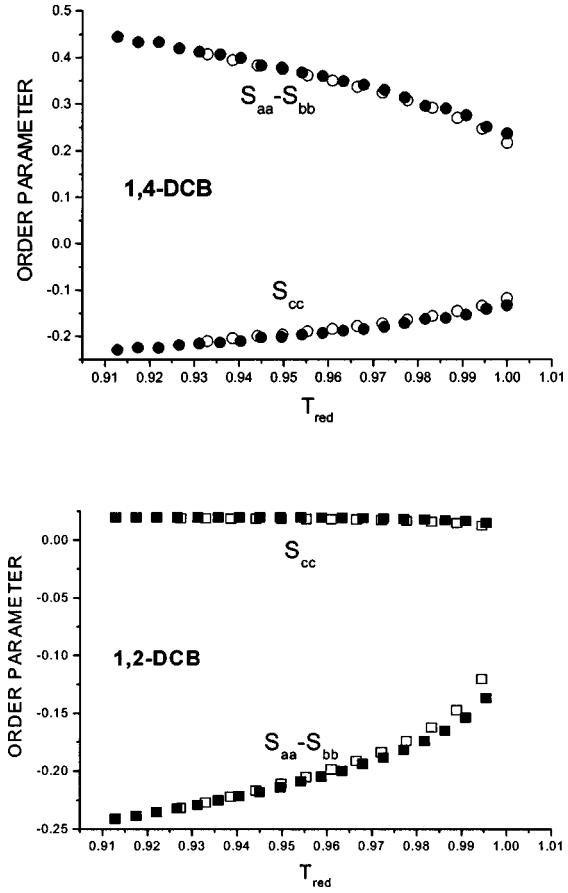

FIG. 5. Temperature dependence of the order parameters S_{cc} and $(S_{aa}-S_{bb})$ as determined directly from the respective experimental splittings of 1,4-DCB in DPDA-C6 (open symbols) and DPDA-OC5 (filled symbols) using Eq. (9) (top) and 1,2-DCB in DPDA-C6 (open symbols) and DPDA-OC5 (filled symbols) using Eq. (10) (bottom).

although the respective splittings (with or without scaling by the solvent order parameter) are appreciably different. This is a result of the particular way in which the order parameters combine to produce the splittings of 1,4-DCB [see Eq. (9)].

TABLE I. Order parameters of S_{aa}, S_{bb}, and S_{cc} of 1,4-DCB and 1,2-DCB in DPDA-C6 at 330 K, evaluated from the dipolar couplings $\pm D$ and the quadrupolar couplings $\pm \Delta\nu_q$. The sign combination associated with the bold-face entries is singled out by molecular modeling and is used in the plots of Fig. 5.

		1,4-DCB		
$\Delta\nu$ (Hz)	D (Hz)	S_{aa}	S_{bb}	S_{cc}
+492	−57.5	**+0.308**	**−0.098**	**−0.210**
−492	−57.5	+0.308	−0.107	−0.201
+492	+57.5	−0.308	+0.107	+0.201
−492	+57.5	−0.308	+0.098	+0.210
		1,2-DCB		
$\Delta\nu_1$ (Hz)	$\Delta\nu_2$ (Hz)	S_{aa}	S_{bb}	S_{cc}
+15000	+6380	+0.108	+0.019	−0.127
+15000	−6380	+0.108	−0.073	−0.035
−15000	+6380	**−0.108**	**+0.073**	**+0.035**
−15000	−6380	−0.108	−0.019	+0.127

IV. SOLVENT–SOLUTE INTERACTION POTENTIAL

We start out with atomistic descriptions of the mesogens and the solutes in order to compute the pair interaction potential U for all solute–solvent separations ($\mathbf{r}$) and relative orientations (ω). We use semiempirical atom–atom potentials (force fields with the hydrogen atoms explicitly included) to produce an energy map for all relative solute–solvent distances and orientations. The computational approximations involve the use of rigid solutes (substituted benzenes) and the assumption that the nematogens adopt a single, low-energy conformation with the pendant chains in their all-*trans* state.

The calculations are performed using the CERIUS[2] molecular modeling package,[43] in conjunction with the Dreiding force field.[32] The functional form of the force field contains bond length, bond angle, bond torsion, van der Waals, and electrostatic energy terms. The Dreiding force field is chosen because of its simplicity and because it is readily available within the CERIUS[2] molecular modeling package. The force field is validated using small molecules that contain the biphenyl and the alkyl groups found in the DPDA-C6 and DPDA-OC5 solvents; it is generally found to provide reliable estimates of both structural and thermodynamic properties. The same force field was used by Binger *et al.*[44,45] for several liquid crystal molecules in order to describe the interactions between the liquid crystal molecules and polymer surfaces. Partial charges are determined by use of the MOPAC molecular orbital package[46] or the Gasteiger electronegativity method.[47] Both calculations yield very similar distributions for the partial charges. The option of turning off all interactions associated with the charge distributions is offered and through that option it becomes possible to have quantitative estimates of the contribution of electrostatic interactions to the ordering mechanism of the solute molecules.

Energy maps of the full potential (U) and of the potential with the charge distributions turned off (U_0) were constructed and used for the calculation of the expansion coefficients in Eqs. (6) and (7) via numerical integration. The results of these calculations showed that the coefficients of rank $l=4$, or higher, contribute marginally to the values of the solute order parameters S_{ab} and can be neglected in a first approximation.

The qualitative picture that emerges from the calculations of energy maps of the full solvent–solute potential U is as follows:

(1) For all solvent–solute combinations the lowest energies are obtained for parallel (face-to-face) configurations of the solvent/solute rings with the ring centers in register, as shown in Fig. 6.
(2) On shifting the ring centers along the solvent para-axis, while holding the solvent/solute rings parallel, the interaction energy increases. The rate of increase depends on the direction of the shift:

(a) For the 1,4-DCB in DPDA-C6 combination, the increase is weak on shifting the solute ring in the direction of the solvent's terminal chain and is much stronger on shifting in the opposite direction, i.e., towards the $-C\equiv C-C\equiv C-$ region.

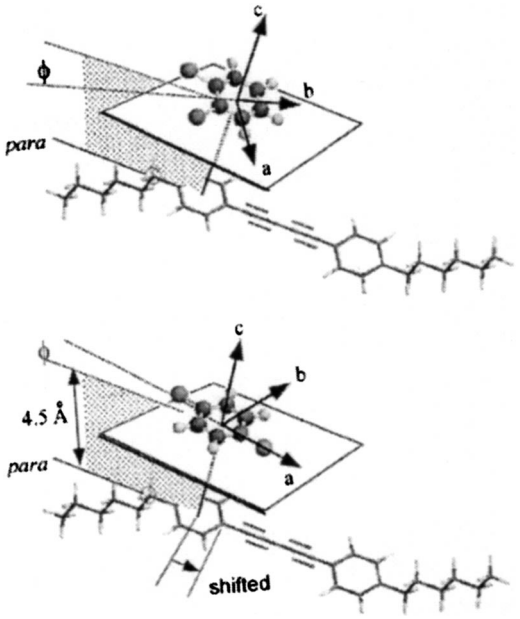

FIG. 6. Schematic representation of solvent–solute configurations showing the parallel-ring configurations and the definition of the azimuthal angle φ for the 1,4-DCB solute (bottom) and the 1,2-DCB solute (top). Two configurations are suggested: One where the solute's *c*-axis intersects a solvent ring's center, called "face-to-face" (F–F; shown), and a second configuration is derived by shifting the solute until its *c*-axis intersects the innermost aromatic carbon of the solvent ring (F–F shifted). The α-methylene of the proximate tail is indicated (small circle) to emphasize that this unit is replaced with an ether linkage for the solvent DPDA-OC5.

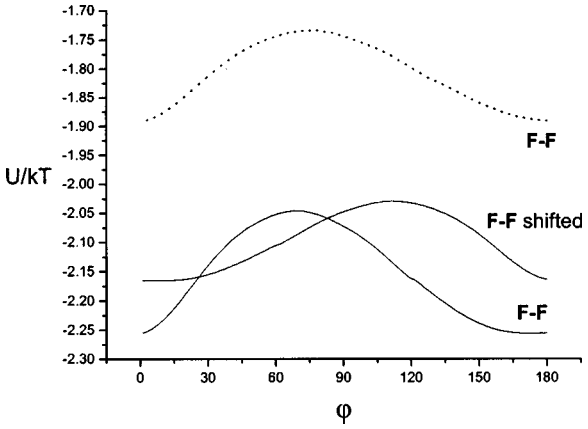

FIG. 7. The dimensionless energy $U(\varphi)$ calculated for 1,4-DCB in DPDA-C6 as a function of the azimuthal angle (φ) between the *a*-axis of the solute and the *para* axis of the solvent (see Fig. 6). Results are shown for two configurations having parallel solute/solvent rings separated by a distance of 4.5 Å: F–F (face-to-face rings), corresponding to aligned ring centers shown in Fig. 6, and a second "F–F shifted" configuration wherein the solute ring center is translated until the solute *c*-axis intersects the solvent's innermost aromatic carbon atom. The dotted line corresponds to the potential $U_0(\phi)$ which differs from $U(\phi)$ in that the electrostatic interactions are turned off.

(b) A different behavior is obtained for the shifted parallel-ring configurations of the 1,4-DCB in DPDA-OC5 combination. Here, the slow increase of the energy values is obtained on shifting the solute rings towards the $-C\equiv C-C\equiv C-$ region and the fast increase is obtained on shifting in the opposite direction, i.e., towards the –O– ether linkage of the solvent. However, on shifting in the same direction past the ether linkage, towards the periphery of the solvent terminal chains, the energy drops to values comparable with those obtained for the $-C\equiv C-C\equiv C-$ region.

(c) Analogous trends of variation on shifting the ring centers are obtained for the energy maps of the 1,2-DCB in each of the two solvents. That is, the variation of the potential with ring-shift shows some qualitative differences in the two solvents but is not particularly sensitive to the molecular structural features that differentiate one solute from the other, namely the relative directions of the dipolar groups.

Turning now to the azimuthal variation of the energy for the parallel solvent/solute ring configurations we find qualitatively similar profiles for the two solutes in the DPDA-C6 solvent but markedly different profiles for each of the solutes in the DPDA-OC5 solvent. In the latter case, the azimuthal profiles are also very sensitive to shifting the solvent/solute ring centers. These features are illustrated on the graphs of the azimuthal dependence of $U(\varphi)$ for the four solvent–solute combinations shown in Figs. 7–10, with the azimuthal angle φ defined in Fig. 6. It is worth noting that:

(1) The sensitivity of $U(\varphi)$ to ring-shifting, shown in Fig. 8, implies fairly strong correlations between azimuthal rotations and translations of the 1,4-DCB solute ring relative to the DPDA-OC5 solvent.

(2) The rather broad (roughly $\pm 50°$) maximum of $U(\varphi)$ shown in Fig. 10 implies strong inhibition of configurations for which the two C–Cl bonds of the 1,2-DCB solute ring are on the same side with the –O– ether linkage of the DPDA-OC5 solvent ring.

(3) On "turning off" the electrostatic interactions, a general overall increase of the energy is obtained for the systems in Figs. 7–9, without significant shifts of the minima. In contrast, for 1,2-DCB in DPDA-OC5 a completely different azimuthal dependence is obtained, as evident from the two curves of Fig. 10.

Having calculated the complete energy maps as described in the beginning of this section, we proceeded to the evaluation of the expansion coefficients C_{lm} according to

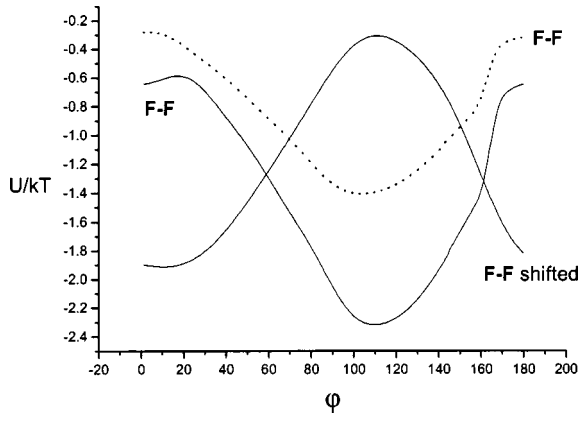

FIG. 8. Same as in Fig. 7 only for 1,4-DCB in DPDA-O5.

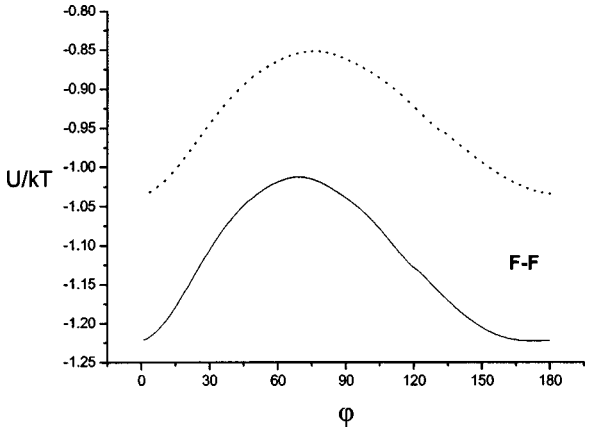

FIG. 9. The dimensionless potential $U(\varphi)$ calculated for 1,2-DCB in DPDA-C6 as a function of the azimuthal angle (φ) relating the symmetry axis (b-axis) of the coplanar solute and the para axis of the solvent rings for configurations separated by a distance of 4.5 Å. F–F (face-to-face rings) corresponding to congruent solute/solvent rings (aligned ring centers, see Fig. 6). The dotted line corresponds to the potential $U_0(\phi)$ which differs from $U(\phi)$ in that the electrostatic interactions are turned off.

Eqs. (6) and (7). The results for the second rank coefficients C_{2m} associated with the four solvet–solute combinations are plotted in Fig. 11 as a function of temperature. These coefficients embody the leading integrated effect that the molecular interaction produces on the orientational tendencies of the solute relative to the solvent molecules. As a result of the choice of the molecular axes frame in relation to the symmetry of the solute molecules, the coefficients with $m=1$ vanish automatically.

Some differences in the behavior of the expansion coefficients for the different solvent–solute combinations should be noted here because of their relevance to the analysis in the next section. In particular, the two solutes are seen to have similar values of C_{22} in the DPDA-C6 solvent but their C_{20} coefficients differ by a factor of 2. Moreover, the relative magnitudes of the coefficients are qualitatively different for the two solutes: the magnitude of C_{20} is somewhat larger than that of C_{22} for 1,4-DCB whereas for the 1,2-DCB solute C_{22} has nearly twice the magnitude of C_{20}. A similar behavior of the relative magnitudes of C_{20} and C_{22} is observed in the DPDA-OC5 solvent except that the temperature dependence, particularly for the coefficients of the 1,4-DCB solute, is different in the two solvents.

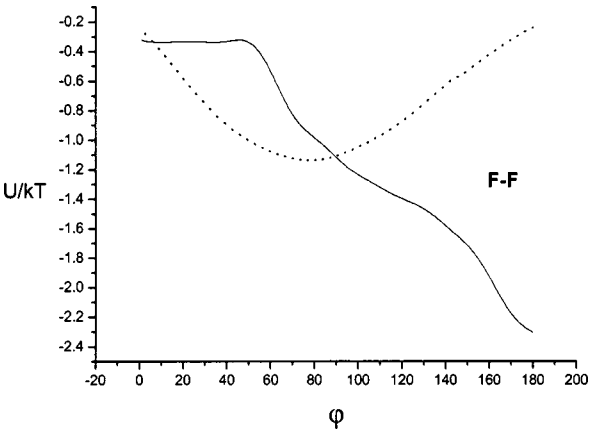

FIG. 10. Same as Fig. 9, only for 1,2-DCB in DPDA-OC5.

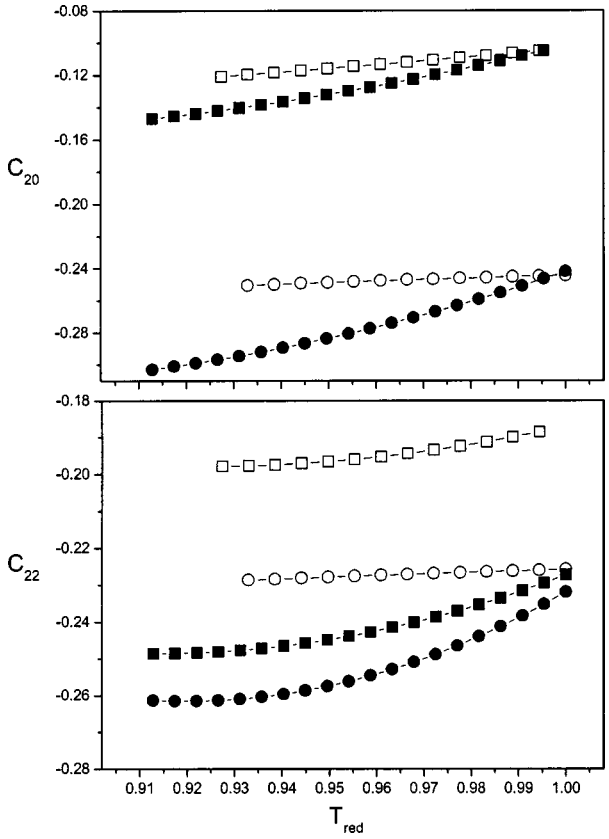

FIG. 11. The temperature dependence of C_{20}-values (top figure) and C_{22}-values [bottom figure, see Eqs. (6) and (7)] for the 1,4-DCB solute in DPDA-C6 (open circles) and DPDA-OC5 (filled circles) and 1,2-DCB solute in DPDA-C6 (open squares) and DPDA-OC5 (filled squares). All coefficients are in units of $C_{00}(T^*)$. The reference temperature T^* is set equal to the temperature of the nematic–isotropic transition T_{NI}.

V. COMPARISON WITH EXPERIMENT AND DISCUSSION

The comparison of the theoretical predictions with experiment is undertaken in two stages. The first stage is concerned with the qualitative aspects: We examine whether the general picture of the solvent–solute interactions described in the previous section is consistent with the basic trends found in the measurements and furthermore whether this picture can help rationalize the experimental results. The second stage deals with the quantitative comparisons of the order parameters obtained from the NMR measurements with those calculated on the basis of the solvent–solute atomistic potential.

At first glance the NMR data for 1,4-DCB seem counterintuitive. In both solvents there is a *decrease* in the 1,4-DCB quadrupolar splitting on lowering the temperature (Fig. 2). Since solvent ordering increases on lowering the temperature in the nematic phases of both DPDA-C6 and DPDA-OC5 (Fig. 2), the observed decrease in $\Delta\nu$ suggests an apparent decrease in solute order at lower temperatures. But this observed trend is merely a consequence of temperature-

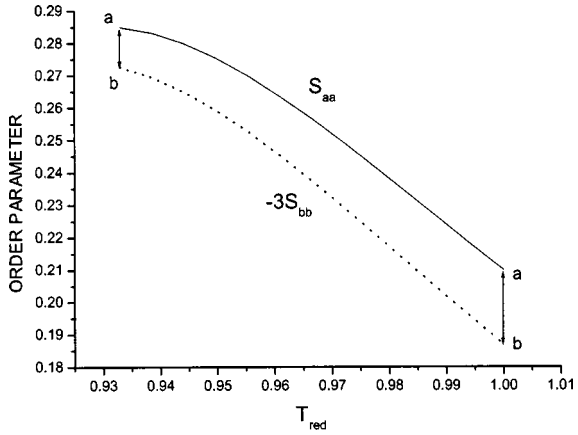

FIG. 12. Calculated order parameters according to Eq. (3) for 1,4-DCB in DPDA-C6 as a function of reduced temperature. The length of the linear segment a–b is proportional to $[S_{aa}+3S_{bb}]$ and is seen to decreases with decreasing temperature.

induced changes in the *magnitude* of a combination of both positive and negative order parameters that describe the quadrupolar splittings.

The final form of Eq. (9) assumes an ideal hexagonal aromatic ring with C–D bonds oriented in the ring plane at $\theta_a=60°$ and $\theta_b=30°$. The inference that $[S_{aa}+3S_{bb}]$ is decreasing as the temperature is lowered is borne out by the calculations: Figure 12 shows plots of the calculated theoretical values for S_{aa} and for $-3S_{bb}$ versus reduced temperature (note S_{bb} is computed to be negative). The gap between these two curves, as measured by the length of the line segment a–b is equivalent to $[S_{aa}+3S_{bb}]$, and, as seen on the graph, a–b decreases with decreasing temperature.

However, to merely suggest that the calculated magnitude of the term $[S_{aa}+3S_{bb}]$ in Eq. (9) is decreasing with temperature because of a nearly complete cancellation of S_{aa} by $3S_{bb}$ contains little information about the preferences for solute ordering in these two closely related solvents. While there are observable differences for the 1,4-DCB solute in the two solvents [Figs. 4(a) and 4(b)], direct examination of the order parameters in both solvents does little to enable a molecular interpretation save for the observation that $S_{aa}>0$, and $S_{bb}<0$. Note, however, this superficial analysis *does* tell us that on average, the 1,4-DCB ring is tangent to the solvent's director ($S_{cc}<0$) since **S** is traceless and $S_{aa}>|S_{bb}|$.

In order to get a deeper microscopic understanding of solute–solvent interactions, one needs to extract from the calculated temperature dependence of S_{aa} and S_{bb} those solute–solvent configurations that dominate U and hence the averaging process detailed in Eqs. (3)–(7). To this end, we return to the qualitative features of the potential energy map outlined in Sec. IV and note that even at this low resolution picture of the energetics of solute–solvent interactions we already begin to see the origin of a negative value for S_{cc}: the coplanar ring configurations bias the solute ring orientation such that the *c*-axis is normal to the mesogen's *para* axis and hence the solute ring remains, on average, tangent to the nematic director. But such coarse categorizations of solute/solvent interaction energies can be further refined in order to begin to develop a more detailed picture of the solute's orientational bias in these two solvents. In the following discussion we focus on the lowest energy configurations—parallel face-to-face solute and solvent rings. In particular, for specific solute–solvent configurations it is instructive to examine the azimuthal angular dependence of $U(\varphi)$ that appears in the calculation of the C_{lm}'s [Eqs. (6) and (7)]. The angle φ is defined via projections on a plane normal to the *c*-axis of the solute (see Fig. 6). For the 1,4-DCB–DPDA-C6 pair depicted in Fig. 6, the angle φ is between the solute's symmetry axis (*a*-axis) and the solvent's ''long axis'' (the para axis of the solvent's rings). The results in Fig. 7 show that for parallel rings, small φ-angles for both coincident ring configurations (F–F) and translated ring configurations (F–F shifted) are energetically more preferable. This observation explains why we find a positive S_{aa} and a negative S_{bb} for 1,4-DCB dissolved in DPDA-C6. Moreover, as the temperature decreases we find that S_{aa} increases in accordance with the result that $U(\varphi=90°)>U(\varphi=0°)$.

The angular dependence of $U(\varphi)$ for the 1,4-DCB in the DPDA-OC5 solvent, illustrated in Fig. 8, reveals a more complex picture. As in the case of DPDA-C6, the lowest energies are achieved for F–F configurations. However, in DPDA-OC5, the F–F configuration with coincident rings shows that the angles near $\varphi=100°$ are energetically more favorable whereas for the translated solute configuration (F–F shifted) low φ-values exhibit lower energy. This energy profile implies competing contributions to S_{aa}. Moreover, this analysis of the dominant solute/solvent configurations shows that for the apolar solute 1,4-DCB, electrostatic contributions to $U(\varphi)$ can be significant: When the charge densities associated with the solute's C–Cl bond and the solute's –O– ether moiety are forced together ($\varphi\rightarrow 0°$), there is a destabilizing contribution to the F–F configuration. Although it might be tempting to attribute this destabilization entirely to electrostatic interactions, inspection of the ''electrostatic-free'' $U_0(\varphi)$ profiles in Fig. 8 shows that the energy minimum around $\varphi=100°$ persists, although with considerably reduced relative depth. This persisting minimum cannot be attributed to steric interactions because it is not present in Fig. 7 where the only molecular structure difference from Fig. 8 is that the –O– ether moiety is replaced by the (not much different in size) $-CH_2-$ unit. This shows that at this level of resolution, the description of ordering in terms of just two kinds of interactions, steric and electrostatic, might be too crude. It is also important to note, here and in similar arguments to follow, that the intermolecular potential U in this detailed atomistic picture is determined by the interaction of the solvent dipole moment with the *individual dipole moments* of the solute and not by the interaction with the overall dipole moment of the solute molecule (that vanishes in the case of 1,4-DCB).

The 1,2-DCB solute ordering, calculated from Eq. (9), in both nematics is clearly different from that exhibited by the 1,4-DCB solute since the 1,2-DCB solute, unlike the 1,4-DCB solute, shows increasing quadrupolar splittings with decreasing T [see Fig. 4(a)]. Although there are coarse similarities between these two solutes' low energy configurations (parallel ring-plane configurations are preferable), the de-

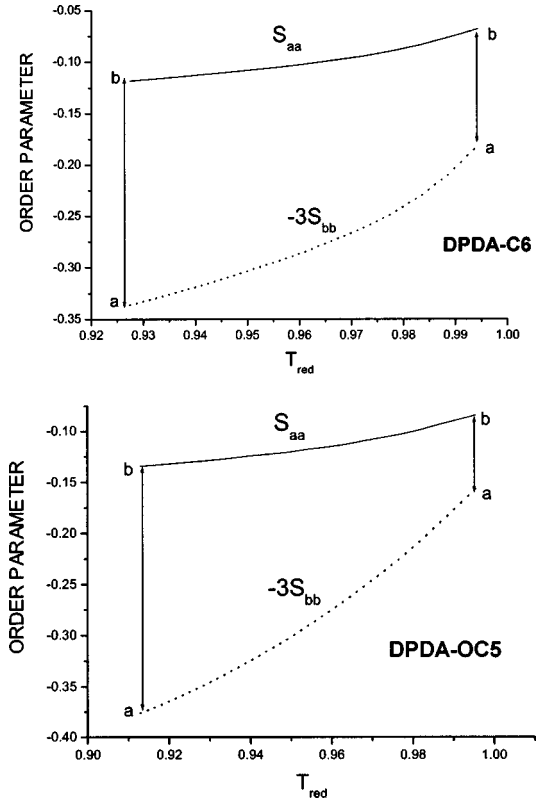

FIG. 13. Calculated order parameters according to Eq. (3) for the 1,2-DCB solute in DPDA-C6 (top) and DPDA-OC5 (bottom) as a function of reduced temperature. The length of the linear segment a–b (proportional to the factor $[S_{aa}+3S_{bb}]$) increases as T decreases.

tailed azimuthal angular dependence shows more extreme behavior in 1,2-DCB (see Figs. 9 and 10). The azimuthal angle for 1,2-DCB is defined by the projection of the solutes symmetry axis (*b*-axis) on the plane (see Fig. 6). For 1,2-DCB in DPDA-C6, the F–F configuration shows a minimum at $\varphi=0°$ (Fig. 9) but the variation of the energy with azimuth is fairly moderate, i.e., all azimuthal orientations are more or less accessible. Nevertheless, the mild energetic bias does imply that S_{bb} is positive and small. By contrast, in DPDA-OC5 (Fig. 10) there is a marked preference for configurations where the dipoles of the solute are away from the polar ether linkage of the solvent ($\varphi>60°$).

The contributions to solute biasing among the parallel-ring configurations described in Figs. 9 and 10 are consonant with the calculated temperature dependence of the order parameters S_{aa} and S_{bb} (Fig. 13). Additionally, the increase in both $\Delta\nu_1$ and $\Delta\nu_2$ with decreasing temperature (Fig. 4) agrees with the increasing magnitude computed for S_{aa} and $[S_{aa}+3S_{bb}]$, respectively, on lowering T [see Eq. (9) and Fig. 13].

The picture emerging from the qualitative analysis of the splittings is supplemented and reinforced by the behavior of the order parameter S_{cc} and the molecular biaxiality order parameter $[S_{aa}-S_{bb}]$ shown in Fig. 5 for the two solutes in both liquid crystal solvents. For the 1,4-DCB solute S_{cc} is significant and negative whereas in the 1,2-DCB solute S_{cc} is close to zero (Fig. 5). This can be understood in terms of excluded volume considerations associated with the low energy azimuthal orientations in the F–F solute–solvent configurations. Angular fluctuations about the 1,4-DCB solutes *b*-axis are inhibited by collisions between the large halogens and the mesogen in the preferred $\varphi=0°$ configuration—disorientation of the *c*-axis relative to the director is impeded. (Note that angular fluctuations about the *a*-axis for this configuration do not disorient the *c*-axis relative to the director.) By contrast, the observation that $S_{cc}\sim 0$ for the 1,2-DCB solute follows from the corresponding argument: In its low energy configuration ($\varphi\sim 180°$), angular fluctuations about the solutes *a*-axis are much less impeded as the pair of chlorines can be readily moved away from the mesogenic core thereby disorienting its *c*-axis relative to the director.

Having rationalized the qualitative behavior of the solute ordering measurements in terms of the underlying solvent–solute interactions, and thereby having established that a quantitative comparison is meaningful, we now turn to such a comparison. To this end we have used the calculated values of the C_{2m} coefficients shown in Fig. 11 to evaluate the respective theoretical splittings according to Eqs. (1)–(7). As indicated in Eq. (5) the values of the order parameters $\langle P_2\rangle$ of the solvent and those of the constants $\eta^*=\overline{\rho}C_{00}(T^*)$ are needed in addition to the values C_{2m}, for determination of the potential of mean torque $V(\omega)$. The $\langle P_2\rangle$ values were obtained directly from the solute order parameter measurements presented in Fig. 2. The η^* values were determined by first calculating $C_{00}(T^*)$ according to Eq. (7) for each solvent–solute pair at the nematic–isotropic transition temperature of the solvent, $T^*=T_{\mathrm{NI}}$, and then determining a (constant) effective number density $\overline{\rho}$ for each solvent by seeking optimal overall agreement of the entire set of calculated quadrupolar splittings, at all temperatures, with the measured values. The so determined constant values of $\overline{\rho}$, which are the sole external parameters in the whole calculation, are $\overline{\rho}=0.0046\ \text{Å}^{-3}$ for the DPDA-C6 solvent and $\overline{\rho}=0.0045\ \text{Å}^{-3}$ for DPDA-OC5.

The calculated theoretical values of the splittings, and comparisons with the measured values presented in Fig. 4(a), are shown for the two solutes in the plots of Figs. 14 and 15. In the same figures are also shown the results of another set of calculations in which all the electrostatic contributions to the solvent–solute intermolecular potential U are removed by ''turning off'' the terms associated with molecular partial charge distributions.

The first noteworthy feature of Figs. 14 and 15 is that the theoretical results are impressively close to experiment, considering that the only adjustable parameters in these calculations are the fixed effective densities of the solvents, i.e., a single, temperature-independent, number for each of the two solvents. Secondly, the removal of the electrostatic component of the solvent–solute interactions is seen in all cases to have a limited effect on the calculated splittings. The effect is more or less temperature independent except for 1,4-DCB in DPDA-C6 where the discrepancy appears to increase with decreasing temperature. It is also interesting to note in Fig. 14 that the electrostatic interactions have opposite effects on the splittings of 1,4-DCB in the two solvents: they show a clear tendency to increase the splitting in DPDA-C6 and to decrease it DPDA-OC5. The reverse tendency is observed

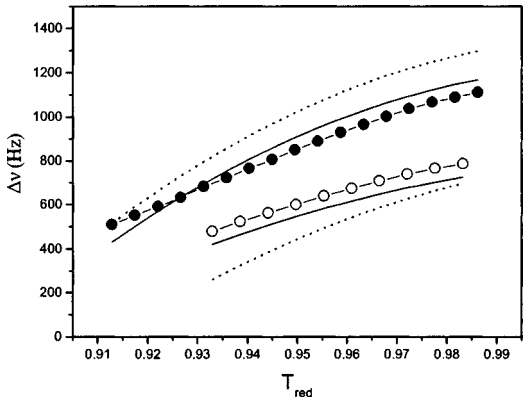

FIG. 14. Calculated splittings, according to Eqs. (1)–(7), as a function of reduced temperature, using the full solvent–solute atomistic potential U (solid lines) and the potential U_0 with partial charge distributions turned off (dotted lines) for the 1,4-DCB solute. For comparison, the experimental data points are also shown (filled circles for the DPDA-OC5 solvent and open circles for DPDA-C6).

for the large splittings ($\Delta\nu_1$) of 1,2-DCB in Fig. 15 and the tendency is inverted once more on going to the small splittings ($\Delta\nu_2$). While it is difficult to gauge from the scale differences in Figs. 14 and 15, the relative discrepancy between experiment and calculated solute quadrupolar splittings (and order parameters) with and without electrostatic interactions is largest for the apolar 1,4-DCB solute both in the polar solvent DPDA-OC5 and in the apolar DPDA-C6 solvent at low temperatures. The removal of the electrostatic interaction of the polar solute 1,2-DCB appears to affect primarily the large splitting in the apolar solvent but in general there is very little difference between calculations with and without electrostatic interactions for the 1,2-DCB; the relative differences between experiment and calculation are about an order of magnitude smaller compared to those of the apolar 1,4-DCB solute.

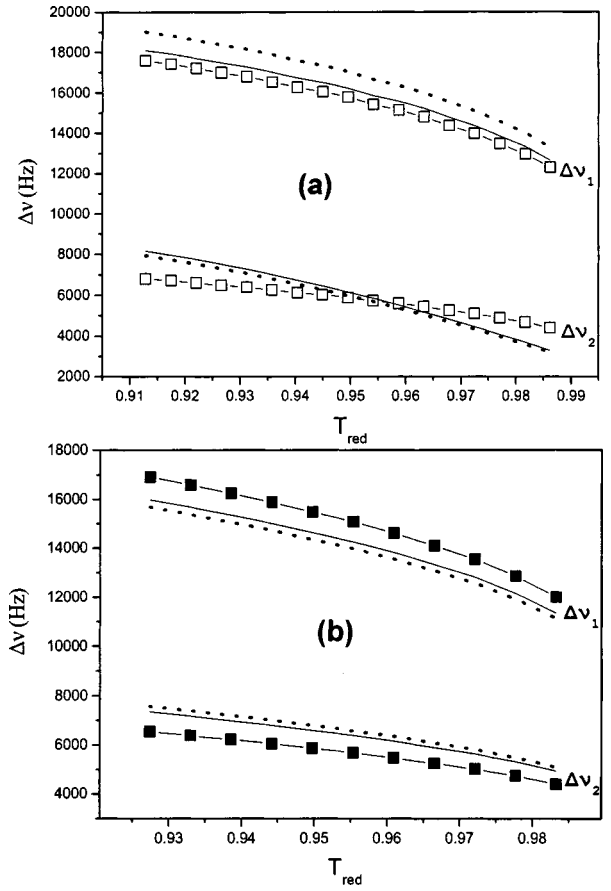

FIG. 15. Calculated splittings, according to Eqs. (1)–(7), as a function of reduced temperature, using the full solvent–solute atomistic potential U (solid lines) and the potential U_0 with partial charge distributions turned off (dotted lines) for the 1,2-DCB solute. For comparison, the experimental data points are also shown (a) filled squares for the DPDA-OC5 solvent and (b) open squares for DPDA-C6.

We close this section by discussing a situation that might at first sight appear paradoxical: Whereas a comparison of Fig. 7 with Fig. 8 (and Fig. 9 with Fig. 10, respectively) shows marked qualitative differences for $U(\varphi)$ in the two solvents, Figs. 4(a), 4(b) and more so, Fig. 5, show very little, if any, effects on the splittings and the order parameters on going from one solvent to the other. Even after the necessary scaling with respect to the solvent order parameter is done [Fig. 4(b)] the quantitative differences in the splittings remain small and the general temperature dependence is qualitatively the same in both solvents. Moreover, the calculated splittings, which are obtained from the potentials that exhibit the qualitatively different azimuthal $U(\varphi)$ profiles in the two solvents, do reproduce very closely the experimental situation, i.e., they show little or practically no ''solvent effect'' in the end. To rationalize this situation it should first be noted that the splittings measured by quadrupolar NMR do not in general provide direct information on the detailed form of the solvent–solute interaction potential; they provide directly only the second moments of the solute orientational distribution $f(\omega)$ which in turn reflects the combined result of weighted sampling of all possible solvent orientations, smeared out by the positional disorder of the nematic phase. It is therefore expected that some features of the interaction may influence the splittings appreciably while the effect of other features may have too weak an influence to be readily identified through the splittings. At a more refined level, these considerations are reinforced with the calculations of the C_{2m} coefficients in Fig. 11: as a result of the position-orientation sampling indicated in Eq. (6), the values of these coefficients for both solutes turn out not to change much from one solvent to the other although the minimum energy configurations of the respective solvent–solute interactions that are being sampled have distinctly different azimuthal dependences. In a simplistic interpretation, the lack of appreciable solvent effects on the splittings could be attributed to nearly identical interactions of the solute molecule with the molecules of the two solvents. However, such interpretation would be far from reality since, as demonstrated explicitly in Sec. III, the interactions with the two solvents are indeed different, and as demonstrated in this section, the manifestations of this difference in the splittings of both 1,4-DCB and 1,2-DCB is simply weakened by the sampling, positional and orientational, of the interactions.

In summary, it would appear that local atomic charge densities and not the overall electrostatic characterization of the solute—polar versus apolar—is critical to an understand-

ing of the role of electrostatic contributions to solute ordering in either polar and apolar nematic solvents.

VI. DISCUSSION AND CONCLUSIONS

Prior to the kind of calculations reported here LC-NMR data from solutes in nematics had limited utility. Frequently one could do little more than tabulate sets of self-consistent order parameters, as in Table I, where the actual solute order parameters (boldface entries) are identified with the help of the modeling we have used. A negative S_{cc} parameter indicates that the solute's phenyl ring plane is tangent to the nematic director (1,4-DCB) but it is usually difficult to go beyond such qualitative characterizations of solute order if the solute–solvent interaction potential U is approximated too coarsely, or, worse, if it is replaced by phenomenological coupling of various solute attributes (shape, electrostatic moments) to respective ''mean fields'' produced by the solvent. In such uniaxial continuum descriptions of nematic solvents,[10,14,15] only approximate forms of the excluded volume interactions are used to construct the orientational distribution of the solute. As a result only empirically-derived treatments of electrostatic interactions are recovered. Moreover, these treatments are suggestive of ways to minimize electrostatic interactions using mixtures of LCs and fail to recognize that solute–solvent interactions even in mixed LCs are solute-dependent. While it is possible in the context of such empirical treatments to select self-consistent sets of order parameters for the solutes we examined, the conclusions about the role of electrostatic contributions to U are necessarily artificial. One can only begin to quantify electrostatic interactions in U by deconvolving these interactions from the excluded volume interactions. However, as long as the latter are dominant and treated approximately, efforts to quantify the electrostatic contributions to solute ordering will be subject to variable error and will be dependent on the model used to approximate the short-range repulsions. In fact, as pointed out in the analysis of the energy profiles of Figs. 7 and 8, even an atomistic description in terms of only steric and electrostatic interactions may not be sufficient to account for certain features of the orientational correlations among solvent–solute molecules and additional atom-specific interactions might be necessary to include in the description.

The work presented here is, to our knowledge, the first report of a fully atomistic theoretical reproduction of the solute orientational order in nematic solvents. The only approximation made in evaluating the solvent–solute molecular interaction is the neglect of molecular polarisabilities by assuming that the molecular partial charge distributions are not modified appreciably as a result of the intermolecular interaction. This constitutes a general limitation of all models based on pairwise additive potentials which, however, did not seem to cause serious quantitative disagreement of the present calculations with experiment. This is partly due to the smallness of the polarizability anisotropy of the solutes compared to that of, say, typical calamitic nematogens.

Our use of an atomistic force field to compute the solvent–solute intermolecular potential as a function of relative orientations and positions has a distinct advantage over calculations that model electrostatic interactions by means of fixed point dipoles and quadrupoles. Additionally, we have the option of switching off the force field's electrostatic interactions. Thus, via computationally consistent comparisons of solute order parameters with and without electrostatic contributions, we demonstrate that it *is* possible to understand in considerable detail the role of the electrostatic interactions in solute ordering in nematics. The collective interactions in the bulk phase were treated in the context of a statistical approximation based on the variational cluster approach where orientational correlations among solvent molecules are compensated for by rescaling the solvent particle density to a fixed, temperature-independent value.

Our theoretical calculations reproduce our experimental results with remarkable accuracy. In addition to the quantitative agreement, the basic features of the atomistic solvent–solute potential provide a clear rationalization of the experimental findings. The influence of the electrostatic contribution on the solute ordering is found to be small for all the solute/solvent pairs studied. Our findings indicate that the important interactions are operative over short intermolecular distances for which the description of the electrostatic component in terms of the leading moments of the overall partial charge of the solvent molecules is not valid. It is explicitly shown that the relevant features of the solvent–solute energy maps are constructed from localized interactions, which are sensitive to the mutual proximity of specific segments of the interacting molecules. The use of the electrostatic moments of the overall molecular charge distribution is of course useful for the description of the electrostatic forces at longer intermolecular separations, but these do not seem to play a significant role in common nematics. Finally, our analysis shows that the practice of treating electrostatic interactions within uniaxial continuum descriptions of the solvent with empirically derived approximations for the solvent–solute potential is too simplistic. Moreover, even if the concept of an ''average electric field gradient'' [10,14] characteristic of each nematic solvent and its putative influence on solute quadrupole moments is viewed in its most primitive role—as a coarse descriptor of the nematic mean field—those critical experimental probes of evidence for such an average field gradient[31] and the results from theory[11] and from computer simulations[30] indicate that the concept is flawed.

ACKNOWLEDGMENTS

This research was supported in part by the National Science Foundation (DMR-9971143). The authors thank Dr. C-D. Poon for help and advice with the NMR experiments. Computational resources for this research were made available by the Graduate Program on Polymer Science and Technology of the University of Patras.

APPENDIX A: DIPHENYLDIACETYLENE MESOGENS

1. Synthesis

The synthesis of both mesogens is shown in Scheme 2. We have slightly adjusted the synthetic route that was used by Grant *et al.*[35,36] The key intermediates 4-*n*-hexyl-

phenylacetylene (**4a**) and 4-*n*-pentyloxyphenylacetylene (**4b**) were obtained in excellent yields by coupling of the appropriate aryl halide (**2a** or **2b**) with (trimethylsilyl)acetylene in the presence of a palladium catalyst.[48]

Scheme 2. Synthetic route to 4,4′-di-*n*-hexyldiphenyldiacetylene (DPDA-C6) (5*a*) and 4,4′-di-*n*-pentyloxydiphenyl diacetylene (DPDA-OC5) (5*b*).

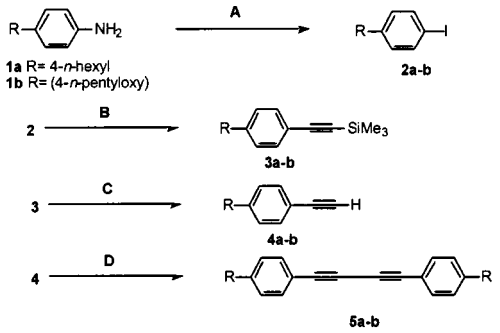

A. 1- HCl/$NaNO_2$, 2- KI/H_2O. *B*. CuI, Et_3N, $Pd(PPH_3)_2Cl_2$, (trimethylsilyl)acetylene, 50 °C *C*. MeOH/NaOH, rt. *D*. DME, CuCl, TMED, O_2.

The trimethylsilyl groups were removed with NaOH in methanol at ambient temperature and the final products (**5a** and **5b**) were obtained by homocoupling of the phenylacetylenes using standard Glaser-coupling conditions.[35]

2. Structure confirmation

The structures of the intermediates and the final products were confirmed by $^1H/^{13}C$ NMR (Varian Gemini 2000-300, 300 MHz). Reactions were monitored by thin layer chromatography using an eluent of hexane/ethyl acetate (9/1). Gas chromatograms (GC) and mass spectra (MS) were obtained with a Hewlett Packard 5890 gas chromatograph and a Hewlett Packard 5972 spectrometer. Infrared spectra were recorded on a Bio-rad FTS-7 spectrometer. The final products (**5a** and **5b**) were dissolved in chloroform and checked for purity using a Waters Integrity HPLC/MS system.

3. Thermal analysis

Transition temperatures were determined by using a Perkin–Elmer DSC-6, calibrated with indium (99.99%) (m.p., 156.5 °C, $\Delta H = 28.315$ J/g). The second heating (10 °C/min) as well as the cooling scans (10 °C/min) were recorded. The DPDA-C6 compound shows a nematic phase from 58 to 85 °C, which is in excellent agreement with the phase behavior reported by Grant.[35] As anticipated we also found a nematic phase for DPDA-OC5, however, the transition temperatures are considerably higher than for DPDA-C6. A crystal to crystal transition is observed at 77 °C, followed by a broad nematic phase from 122 to 159 °C. The second heating of both compounds is shown in Fig. 16.

We also investigated blends of DPDA-C6 and DPDA-OC5. The only mixtures that were miscible contained between 80%–100% DPDA-C6. A mixture of 80% DPDA-C6/20% DPDA-OC5 shows the following phase behavior: (K–N) at 59.34 °C ($\Delta H = 30.06$ J/g) and (N–I) at 97.25 °C ($\Delta H = 2.26$ J/g).

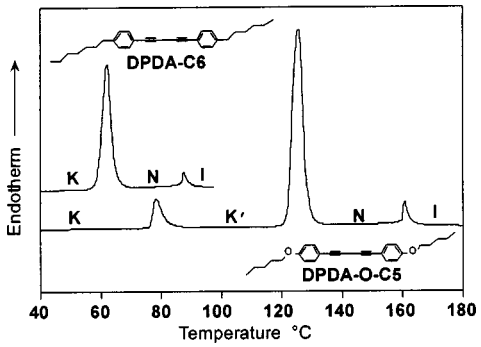

FIG. 16. DSC trace of DPDA-C6 with DPDA-OC5. Second heating with 10 °C/min.

4. Optical microscopy

The phase behavior of DPDA-C6 and DPDA-OC5 was characterized using polarizing microscopy (Nikon Microphot-FX polarizing microscope equipped with a Linkham hotstage). Samples were studied between glass slides using heating and cooling rates of 10 °C/min. Both compounds exhibit typical nematic schlieren textures with both integer and half-integer disclinations (four brushes, $S = \pm 1$ and two brushes, $S = \pm 1/2$).

APPENDIX B: SYNTHESIS

4-*n*-hexyloxyaniline, 4-*n*-pentyloxyaniline, bis(triphenylphosphine)palladium dichloride, (trimethylsilyl)acetylene, 1,4-dichlorobenzene-d_4, and 1,2-dichlorobenzene-d_4 were purchased from Aldrich Chemical Co. and used as received. Triethylamine and dimethoxyethane (DME) were dried over and distilled from calcium hydride prior to use. *N*,*N*,*N*′,*N*′-Tetramethylethylenediamine (TMED) was treated with a small amount of 1.0 M *n*-BuLi in hexanes and purified by vacuum distillation.[49]

1. 4-*n*-Hexyl-iodobenzene (2a)

A mechanically stirred mixture of 4-*n*-hexylaniline (25 g, 0.141 mol) and 36% HCl (110 ml) was cooled to −5 °C. A solution of $NaNO_2$ (11.54 g, 0.167 mol) in 60 ml H_2O was cooled to 0 °C and slowly added while maintaining the temperature at −5 °C. The final solution was stirred at 0 °C for 30 min. A solution of KI (46.1 g, 0.278 mol) in 60 ml H_2O was added dropwise keeping the temperature between 0–5 °C. The resulting mixture was stirred overnight and extracted twice with ethylether. The organic layer was consecutively washed with a concentrated sodium metasulphite solution, 5% NaOH, water and dried over $MgSO_4$. The solvent was removed under reduced pressure and the crude product was purified by vacuum distillation. 4-*n*-hexyl-iodobenzene was obtained as a slight yellow liquid at 110 °C/50 mTorr. Yield 26.4 g (65%). GC tr=10.3 min, MS (*m*/*z*): 288 (M+), 217, 91.

2. Analytical data of 4-(*n*-pentyloxy)-iodobenzene (2b)

4-(*n*-pentyloxy)-iodobenzene was obtained as a yellow liquid at 110 °C/450 mTorr. Yield 22.23 g (55%). GC tr =10.5 min, MS (*m*/*z*): 290 (M+), 220, 93, 65.

3. 4-*n*-hexylphenylacetylene (4a)

To a solution of 4-*n*-hexyl-iodobenzene (21.44 g, 0.0744 mol), $Pd(PPh_3)_2Cl_2$ (1.302 g, 1.9 mmol), and CuI (0.141 g, 0.7 mmol) in 200 ml triethylamine was added (trimethylsilyl)acetylene (8.04 g, 0.0818 mol). This mixture was stirred at 50 °C for 4 h and cooled to room temperature and the gray salt was removed by filtration. The solvent was removed under reduced pressure and the resulting dark red oil was dissolved in hexane and filtered over a short pad of silicagel/celite. The solvent was removed under reduced pressure and the crude trimethylsilyl(4-*n*-hexylphenyl)acetylene (**3a**) was chromatographed over silica gel (hexane/ethyl acetate 9:1).

A solution of **3a** (5.0 g, 0.02 mol) in 100 ml methanol was treated with NaOH (0.25 g, 0.005 mol) at room temperature. After 4 h the solvent was removed and the residue dissolved in diethylether. The organic layer was washed with 5% $NaHCO_3$ and dried over $MgSO_4$. The solvent was removed and the crude product was purified using a kugelrohr apparatus. 4-*n*-hexylphenylacetylene was obtained as a clear oil at 80 °C/200 mTorr. Yield: 3.4 g (91%). ^{1}H NMR (300 MHz, $CDCl_3$) δ 0.89 (t,J=7 Hz,3H), 1.2–1.4 (m, 6H), 1.55–1.7 (m, 2H), 2.59 (t,J=8 Hz,2H), 3.02 (s, 1H), 7.12 (d,J=9 Hz,2H), 7.40 (d,J=8 Hz,2H); ^{13}C NMR (75.46 MHz, $CDCl_3$) δ: 14.08 (ω-$\underline{C}H_3$), 22.58 (ε-$\underline{C}H_2$), 29.89 (γ-$\underline{C}H_2$), 31.17 (β-$\underline{C}H_2$), 31.67 (δ-$\underline{C}H_2$), 35.87 (α-$\underline{C}H_2$), 76.39 (C1), 83.83 (C2), 119.1 (C3), 128.3 (C5), 132.0 (C4), 143.9 (C6).

4. Analytical data of 4-(*n*-pentyloxy)acetylene (4b)

4-(*n*-pentyloxy)acetylene was obtained as a yellow liquid at 110 °C/450 mTorr. Yield 7.2 g (90%). ^{1}H NMR (300 MHz, $CDCl_3$) δ0.91 (t,J=7 Hz,3H), 1.3–1.5 (m, 4H), 1.7–1.83 (m, 2H), 2.97 (s, 1H), 3.92 (t,J=6 Hz,2H), 6.80 (d,J=9 Hz,2H), 7.39 (d,J=8 Hz,2H); ^{13}C NMR (75.46 MHz, $CDCl_3$) δ: 13.97 (ω-$\underline{C}H_3$), 22.4 (ε-$\underline{C}H_2$), 28.1 (γ-$\underline{C}H_2$), 28.81 (β-$\underline{C}H_2$), 34.98 (δ-$\underline{C}H_2$), (α-$\underline{C}H_2$), 67.95 (C1), 83.68 (C2), 113.8 (C3), 114.3 (C5), 133.4 (C4), 159.4 (C6).

5. 4,4′-di-*n*-hexyldiphenyldiacetylene (DPDA-C6) (5a)

Oxygen was bubbled vigorously through a bright blue solution of cuprous chloride (0.4 g, 4 mmol) and TMED (0.8 g, 6.8 mmol) in 40 ml DME at 35 °C. The solution immediately turned bright green and a solution of 4-*n*-hexylphenylacetylene (**4a**) (3.7 g, 20 mmol) in 20 ml DME was added dropwise. The reaction mixture was allowed to stir for 1.5 h at room temperature. A dilute HCl solution (80 ml, 2%) was slowly added and the aqueous phase was extracted three times with ethyl ether, washed with water, and dried over $MgSO_4$. The solvent was removed by distillation and the crude product was recrystallized from MeOH. Yield: 1.34 g (36%). HPLC: t_r=4.84 min (98%). ^{1}H NMR (300 MHz, $CDCl_3$) δ0.87 (t,J=7 Hz,3H), 1.2–1.4 (m, 6H), 1.59 (m, 2H), 2.59 (t,J=8 Hz,2H), 7.13 (d,J=8 Hz,2H), 7.41 (d,J=8 Hz,2H); ^{13}C NMR (75.46 MHz, $CDCl_3$) δ: 14.02 (ω-$\underline{C}H_3$), 22.51 (ε-$\underline{C}H_2$), 28.85 (γ-$\underline{C}H_2$), 31.07 (β-$\underline{C}H_2$), 31.6 (δ-$\underline{C}H_2$), 35.92 (α-$\underline{C}H_2$), 73.39 (C1), 81.5 (C2), 118.9 (C3), 128.5 (C5), 132.3(C4), 144.4(C6). IR (KBr) ν_{max}: 2150 (alkyne), 1653, 1601, 1559, 1506, 1458, 1175, 1018, 844, 838, 819 cm^{-1}.

6. Analytical data of 4,4′-di-*n*-pentyloxydiphenyldiacetylene (DPDA-OC5) (5b)

Yield: 3.25 g (77%), recrystallized from EtOH. HPLC: t_r=21.64 min (99%). ^{1}H NMR (300 MHz, $CDCl_3$) δ 0.91 (t,J=7 Hz,3H), 1.3–1.5 (m, 4H), 1.76 (m, 2H), 3.93 (t,J=7 Hz,2H), 6.81 (d,J=9 Hz,2H), 7.42 (d,J=9 Hz,2H); ^{13}C NMR (75.46 MHz, $CDCl_3$) δ: 14.16 (ω-$\underline{C}H_3$), 22.58 (δ-$\underline{C}H_2$), 28.28 (γ-$\underline{C}H_2$), 28.97 (β-$\underline{C}H_2$), 68.21 (α-$\underline{C}H_2$), 73 (C1), 81.43 (C2), 113.7 (C3), 114.7 (C5), 134.1 (C4), 159.9 (C6). IR (KBr) ν_{max} 2155 (alkyne), 1653, 1600, 1559, 1506, 1473, 1388, 1291, 1254, 1174, 1109, 1019, 831, 806 cm^{-1}.

[1] A. Saupe and G. Englert, Phys. Rev. Lett. **11**, 462 (1963).
[2] S. Meiboom and L. C. Snyder, Science **162**, 1337 (1968).
[3] For an entre to this literature see, C. I. Khetrapal, G. A. Negana Gowda, and K. V. Ramanathan, *Nuclear Magnetic Resonance*, edited by G. A. Webb (Specialist Periodical Reports) (Royal Society of Chemistry, Cambridge, 2002), Vol. 31.
[4] Z. Luz and S. Meiboom, J. Chem. Phys. **59**, 275 (1973).
[5] D. Goldfarb, Z. Luz, and H. Zimmermann, Isr. J. Chem. **23**, 341 (1983).
[6] J. Charvolin and Y. Hendrikx, in *Nuclear Magnetic Resonance of Liquid Crystals*, edited by J. W. Emsley, NATO ASI Series C (Reidel, Dordrecht, 1985), Vol. 141, p. 449.
[7] J. W. Emsley, in Ref. 6, p. 379.
[8] R. Y. Dong, *Nuclear Magnetic Resonance of Liquid Crystals* (Springer-Verlag, New York, 1997).
[9] M. Zweckstetter and A. Bax, J. Am. Chem. Soc. **123**, 9490 (2001); F. Tian, H. Valafar, and J. H. Prestegard, *ibid.* **123**, 11791 (2001).
[10] E. E. Burnell and C. de Lange, Chem. Rev. **98**, 2359 (1998).
[11] A. F. Terzis and D. J. Photinos, Mol. Phys. **83**, 847 (1994).
[12] W. M. Gelbart, J. Phys. Chem. **86**, 4298 (1982).
[13] A. F. Terzis, C.-D. Poon, E. T. Samulski, Z. Luz, R. Poupko, H. Zimmermann, K. Müller, H. Toriumi, and D. J. Photinos, J. Am. Chem. Soc. **118**, 2226 (1996).
[14] R. T. Syvitski and E. E. Burnell, J. Chem. Phys. **113**, 3452 (2000).
[15] M. Y. Kok, A. J. Van der Est, and E. E. Burnell, Liq. Cryst. **3**, 485 (1988).
[16] J. W. Emsley, W. E. Palke, and G. N. Shilstone, Liq. Cryst. **9**, 643 (1991).
[17] D. J. Photinos, C. D. Poon, E. T. Samulski, and H. Toriumi, J. Phys. Chem. **96**, 8176 (1992).
[18] D. J. Photinos and E. T. Samulski, J. Chem. Phys. **98**, 10009 (1993).
[19] M. E. van Leeuwen and B. Smit, Phys. Rev. Lett. **69**, 913 (1993).
[20] J. J. Weis, D. Levesque, and G. J. Zarragoicoechea, Phys. Rev. Lett. **69**, 913 (1993).
[21] R. P. Sear, Phys. Rev. Lett. **76**, 2310 (1996).
[22] S. C. NcGrother, A. Gil-Villega, and G. Jackson, J. Phys.: Condens. Matter **8**, 9649 (1996).
[23] R. Berardi, M. Ricci, and C. Zannoni, Phys. Chem. Chem. Phys. **2**, 443 (2001).
[24] A. G. Vanakaras and D. J. Photinos, Mol. Phys. **85**, 1089 (1995).
[25] D. A. Dunmur and K. Toriyama, Liq. Cryst. **1**, 169 (1988).
[26] W. H. de Jeu, Philos. Trans. R. Soc. London, Ser. A **309**, 217 (1983).
[27] P. E. Cladis, Mol. Cryst. Liq. Cryst. **165**, 85 (1988).
[28] F. Hardouin, A. M. Levelut, and G. Sigaud, Solid State Commun. **33**, 337 (1980).
[29] R. Berardi, S. Orlandi, D. J. Photinos, A. G. Vanakaras, and C. Zannoni, Phys. Chem. Chem. Phys. **4**, 770 (2002).
[30] E. E. Burnell, R. Berardi, R. T. Syvitski, and C. Zannoni, Chem. Phys. Lett. **331**, 455 (2000).
[31] J. Jokisaari, P. Ingman, J. Lounila, O. Pulkkinen, P. Diehl, and O. Muenster, Mol. Phys. **78**, 41 (1993).
[32] S. L. Mayo, B. D. Olafson, and W. A. Goddard, J. Phys. Chem. **94**, 8897 (1990).

[33] J. W. Emsley and J. C. Lindon, *NMR Spectroscopy Using Liquid Crystals* (Pergamon, New York, 1965).
[34] G. R. Luckhurst and G. W. Gray, *The Molecular Physics of Liquid Crystals* (Academic, New York, 1979).
[35] B. Grant, Mol. Cryst. Liq. Cryst. **48**, 175 (1978).
[36] B. Grant, N. J. Clecak, and R. J. Cox, Mol. Cryst. Liq. Cryst. **51**, 209 (1979).
[37] B. Fung and J. Afzal, J. Am. Chem. Soc. **108**, 1107 (1986).
[38] D. P. Burum, M. Linder, and R. R. Ernst, J. Magn. Reson. (1969–1992) **44**, 173 (1981).
[39] J. Courtieu, D. W. Alderman, and D. M. Grant, J. Am. Chem. Soc. **103**, 6783 (1981).
[40] C.-D. Poon and B. M. Fung, J. Chem. Phys. **91**, 7392 (1989).
[41] Z. Luz, R. C. Hewitt, and S. Meiboom, J. Chem. Phys. **61**, 1758 (1974).
[42] R. Poupko, R. L. Vold, and R. R. Vold, J. Magn. Reson. **34**, 67 (1979).
[43] CERIUS^2 v.4.1, Molecular Modelling Software, available from Accelrys Ltd., 230/250 The Quorum Barnwell Road, Cambridge CB5 8RE, United Kingdom (www.accelrys.com).
[44] D. R. Binger and S. Hanna, Liq. Cryst. **26**, 1205 (1999).
[45] D. R. Binger and S. Hanna, Liq. Cryst. **27**, 89 (2000).
[46] J. J. P. Stewart, J. Comput.-Aided Mol. Des. **4**, 1 (1999).
[47] J. Gasteiger and M. Marsili, Tetrahedron **36**, 3219 (1979).
[48] J. Lu, T. Minquan, Q. Chen, and J. Wen Wen, Liq. Cryst. **18**, 101 (1995).
[49] D. D. Perrin and W. L. F. Armarego, *Purification of Laboratory Chemicals* (Pergamon, New York, 1988), p. 286.